

Article

Interplay of Experiment and Theory in Elucidating Mechanisms of Oxidation Reactions by a Nonheme RuO Complex

Sunder N. Dhuri, Kyung-Bin Cho, Yong-Min Lee, Sun Young Shin,
Jin Hwa Kim, Debasish Mandal, Sason Shaik, and Wonwoo Nam

J. Am. Chem. Soc., **Just Accepted Manuscript** • DOI: 10.1021/jacs.5b04787 • Publication Date (Web): 15 Jun 2015

Downloaded from <http://pubs.acs.org> on June 18, 2015

Just Accepted

“Just Accepted” manuscripts have been peer-reviewed and accepted for publication. They are posted online prior to technical editing, formatting for publication and author proofing. The American Chemical Society provides “Just Accepted” as a free service to the research community to expedite the dissemination of scientific material as soon as possible after acceptance. “Just Accepted” manuscripts appear in full in PDF format accompanied by an HTML abstract. “Just Accepted” manuscripts have been fully peer reviewed, but should not be considered the official version of record. They are accessible to all readers and citable by the Digital Object Identifier (DOI®). “Just Accepted” is an optional service offered to authors. Therefore, the “Just Accepted” Web site may not include all articles that will be published in the journal. After a manuscript is technically edited and formatted, it will be removed from the “Just Accepted” Web site and published as an ASAP article. Note that technical editing may introduce minor changes to the manuscript text and/or graphics which could affect content, and all legal disclaimers and ethical guidelines that apply to the journal pertain. ACS cannot be held responsible for errors or consequences arising from the use of information contained in these “Just Accepted” manuscripts.

Interplay of Experiment and Theory in Elucidating Mechanisms of Oxidation Reactions by a Nonheme Ru^{IV}O Complex

Sunder N. Dhuri,^{†,‡,§} Kyung-Bin Cho,^{†,§} Yong-Min Lee,[†] Sun Young Shin,[†] Jin Hwa Kim,[†] Debasish Mandal,[¶] Sason Shaik,[¶] Wonwoo Nam^{†,*}

[†] Department of Chemistry and Nano Science, Ewha Womans University, Seoul 120-750, Korea

[‡] Department of Chemistry, Goa University, Goa 403 206, India

[¶] Institute of Chemistry and the Lise Meitner-Minerva Center for Computational Quantum Chemistry, The Hebrew University of Jerusalem, 91904 Jerusalem, Israel

ABSTRACT: A comprehensive study on the reactivity patterns and reaction mechanisms in alkane hydroxylation, olefin epoxidation, cyclohexene oxidation, and sulfoxidation reactions by a mononuclear nonheme ruthenium(IV)-oxo complex, [Ru^{IV}(O)(terpy)(bpm)]²⁺ (**1**), has been conducted experimentally and theoretically. In alkane hydroxylation (i.e., oxygen rebound versus oxygen non-rebound mechanisms), both the experimental and theoretical results show that the substrate radical formed via a rate-determining hydrogen atom (H-atom) abstraction of alkanes by **1** prefers dissociation over oxygen rebound and desaturation processes. In the oxidation of olefins by **1**, the observations of the kinetic isotope effect (KIE) value of 1 and the styrene oxide formation lead us to conclude that an epoxidation reaction via an oxygen atom transfer (OAT) from the Ru^{IV}O complex to the C=C double bond is the dominant pathway. DFT calculations show that the epoxidation reaction is a two-step two-spin state process. In contrast, the oxidation of cyclohexene by **1** affords products derived from the allylic C-H bond oxidation, with a high KIE value of 38(3). The preference of the H-atom abstraction over the C=C double bond epoxidation in the oxidation of cyclohexene by **1** is elucidated by DFT calculations, in which the C-H activation energy barrier is 4.5 kcal mol⁻¹ lower than the epoxidation energy barrier. In the oxidation of sulfides, the sulfoxidation by the electrophilic Ru-oxo group of **1** occurs via a direct OAT mechanism, and DFT calculations show that this is a two-spin state reaction where the transition state is the lowest in the *S* = 0 state.

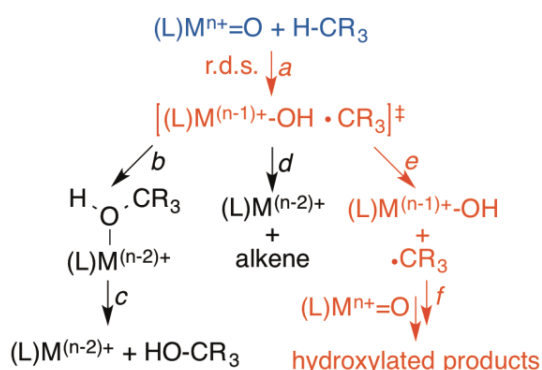
INTRODUCTION

High-valent metal-oxo complexes of heme and nonheme ligands perform a wide range of biological oxidation reactions, such as alkane hydroxylation, olefin epoxidation, and sulfoxidation.¹⁻¹⁰ The reactivities and reaction mechanisms of the metal-oxo complexes have been investigated intensively over the past several decades due to their tremendous potential for industrial and biomimetic uses. For example, a large number of high-valent Fe^{IV}O complexes have been synthesized and investigated in heme and nonheme systems, and their chemical and reactivity properties have been well established resulting from intensive mechanistic studies, including as for the C-H bond activation reactions of alkanes occurring via an hydrogen atom (H-atom) abstraction (Scheme 1A), C-H bond activation or epoxidation reactions of olefins (Schemes 1B and 1C), and oxidation reactions of sulfides (Scheme 1C).¹¹⁻¹⁶

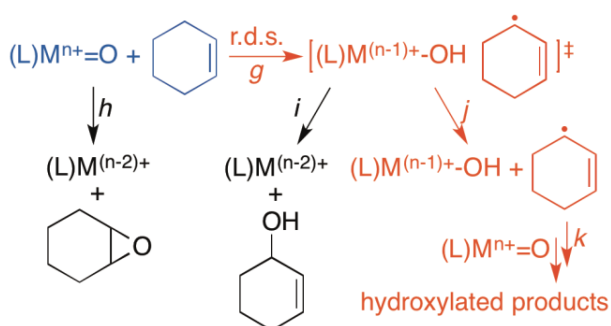
High-valent ruthenium-oxo complexes of heme and nonheme ligands have also been invoked as active oxidants in catalytic oxidation reactions.¹⁷⁻¹⁹ In heme models, Ru-oxo porphyrin (Por) species have been shown to perform C-H bond activation of alkanes, most likely by (Por)Ru^VO species, which are the Ru analogues of the CYP450 Compound I species.²⁰⁻²³ The oxidation reactions of alkanes and olefins by nonheme Ru complexes have long been known as well, wherein certain organic products were formed selectively in high yields.²⁴⁻⁴⁷ Such reactions are known to occur via H-atom abstraction, hydride transfer, electron transfer, proton-coupled electron transfer (PCET), or oxygen atom transfer (OAT) mechanisms. For instance, oxidation of cumene by *cis*-[Ru^{IV}(bpy)(py)(O)]²⁺ (bpy = 2,2'-bipyridyl, py = pyridine) was first investigated several decades ago.²⁵ It was initially thought to occur through a hydride transfer mechanism,²⁵ but it was later shown to occur through a H-atom abstraction mechanism.³⁵ One of the suggested pathways

Scheme 1. Proposed Mechanisms in Alkane Hydroxylation, Cyclohexene Oxidation, and Oxygen Atom Transfer Reactions by Metal-Oxo Species

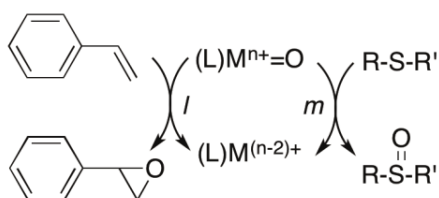
A. Alkane hydroxylation by (L)Mⁿ⁺=O



B. Oxidation of cyclohexene by (L)Mⁿ⁺=O



C. Oxygen atom transfer reactions by (L)Mⁿ⁺=O



included a cumyl radical reacting with a second Ru^{IV}O species (Scheme 1A, pathways a, e, and f). As multiple organic products were seen in this reaction, as well as Ru^{II} products, it was concluded that this pathway acts parallel to oxygen rebound and desaturation type reactions done by Ru^{III}OH (Scheme 1A, pathways b, d, and e), followed by more downstream reactions in the pathway to the final products. A second example, also using cumene as a substrate but with different catalyst ligands, resulted in experimental observation of Ru^{III}OH and Ru^{III}-alkoxo species, described as intermediates of a rebound process (Scheme 1A, pathways a, b, and c).⁴⁵ A third example is the oxidation of cyclohexene and indene, which was likewise shown to occur through an initial C-H bond activation pathway rather than an epoxidation pathway (Scheme 1B, pathways g versus h).³² The reactions were

proposed to occur through many pathways that ultimately accounted for the formation of different organic products, kinetics, and spectra related to the reactions. Other substrates were also used in the mechanistic studies of Ru^{IV}O complexes.^{30,33-37}

Although tremendous efforts have been made to elucidate the mechanism(s) of C-H bond activation of benzylic and allylic C-H bonds by Ru^{IV}O species,^{24,28,29,31,32,34,35} theoretical studies have been underused to decipher the distinct mechanistic steps of bond activation by Ru^{IV}O. While there are some pure theoretical works in Ru-oxo chemistry (e.g., using (Por)Ru^{VO} species),^{22,23} combined experimental and theoretical studies give a much more powerful insight into reaction mechanisms, as shown by our earlier work on the fundamental differences between two-state and single-state reactivity patterns of Fe^{IV}O and Ru^{IV}O complexes in the C-H bond activation reactions.⁴⁸ Furthermore, combining experimental and theoretical methods have enabled us to establish that the mechanism of the C-H bond activation of hydrocarbons by metal-oxo species in nonheme synthetic model reactions is different from the oxygen rebound mechanism that has been well established in heme enzymes and their models. In the oxygen rebound mechanism, the H-atom abstraction results in the formation of a carbon radical and a metal-hydroxo complex (Scheme 1A, pathway a), followed by the rebound of the carbon radical to the metal-hydroxo that results in producing alcohol or desaturated products (Scheme 1A, pathways b, c, and d).⁴⁹⁻⁵³ However, in the case of a dissociative oxygen non-rebound reaction, the substrate radical escapes from the cage and then reacts with a second metal-oxo molecule to give hydroxylated products (Scheme 1A, pathways e and f for alkane hydroxylation; Scheme 1B, pathways j and k for allylic C-H bond activation).⁵⁴⁻⁵⁹ We have shown recently that this radical dissociative mechanism prevails in C-H bond activation reactions by Fe^{IV}O, Mn^{IV}O, Cr^{IV}O, and Fe^VO catalysts in nonheme systems.⁵⁴⁻⁵⁹ Very recently, we have also shown that an interplay of tunneling and spin inversion probability has to be taken into account in

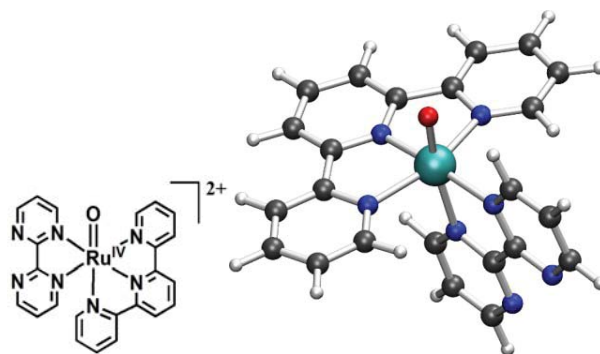


Figure 1. Chemical structure (left) and DFT-optimized structure (right) of complex **1**, optimized at B3LYP/LACVP level. Atom colors: ● = Ru, ● = O, ● = N, ● = C, and ● = H.

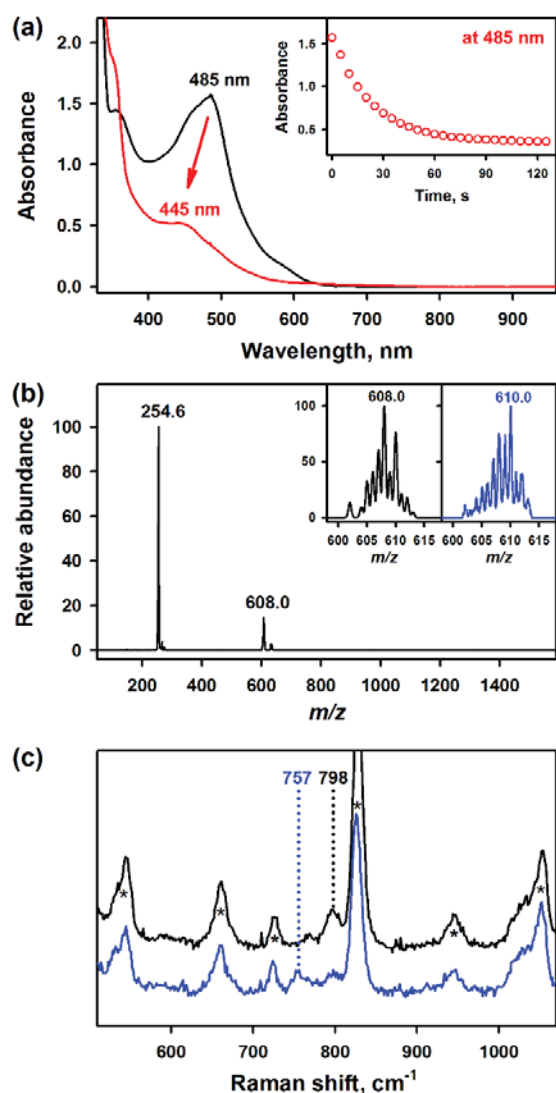


Figure 2. (a) UV-vis spectra of $[\text{Ru}(\text{terpy})(\text{bpm})(\text{H}_2\text{O})]^{2+}$ (0.25 mM, black line) and **1** (0.25 mM, red line) in CH_3CN at 25 °C. Inset shows the time course monitored at 485 nm due to the decay of $[\text{Ru}(\text{terpy})(\text{bpm})(\text{H}_2\text{O})]^{2+}$. (b) ESI-MS of **1**. Peaks at $m/z = 254.6$ and 608.0 correspond to $[\text{Ru}^{\text{IV}}(\text{O})(\text{terpy})(\text{bpm})]^{2+}$ (calc. $m/z = 254.5$) and $[\text{Ru}^{\text{IV}}(\text{O})(\text{terpy})(\text{bpm})(\text{ClO}_4)]^+$ (calc. $m/z = 608.0$), respectively. Insets show the observed isotope distribution patterns for $1\text{-}^{16}\text{O}$ at $m/z = 608.0$ (left panel) and $1\text{-}^{18}\text{O}$ at $m/z = 610.0$ (right panel). (c) Resonance Raman spectra of $1\text{-}^{16}\text{O}$ (black line) and $1\text{-}^{18}\text{O}$ (blue line) in CH_3CN recorded with 406.7-nm modeling this kind of C-H activation reactions.⁵⁹

Herein, we provide results obtained from combined experimental and theoretical studies that strongly support that the C-H bond activation of alkanes by a mononuclear nonheme $\text{Ru}^{\text{IV}}\text{O}$ complex, $[\text{Ru}^{\text{IV}}(\text{O})(\text{terpy})(\text{bpm})]^{2+}$ (**1**, terpy = 2,2':6',2''-terpyridine, bpm = 2,2'-bipyrimidine; see Figure 1 for DFT-optimized structure), follows a dissociative oxygen non-rebound mechanism (Scheme 1A, reaction pathway e). While the

oxidation of styrene and thioanisole by **1** occurs via an OAT mechanism, we show that the oxidation of cyclohexene by **1** affords products resulted from a C-H bond activation reaction rather than an epoxidation reaction. All the results obtained experimentally in this study are replicated in silico by theoretical calculations, detailing the precise steps involved in the oxidation reactions.

RESULTS AND DISCUSSION

Generation and Characterization of 1. The ruthenium(IV)-oxo complex **1** was synthesized by reacting $[\text{Ru}^{\text{II}}(\text{terpy})(\text{bpm})(\text{H}_2\text{O})](\text{ClO}_4)_2$ with PhIO in CH_3CN at 25 °C.⁶⁰ Upon addition of PhIO (1.2 equiv, dissolved in MeOH) to a solution containing the starting Ru^{II} complex, the UV-vis band at 485 nm decayed within 2 min with the concurrent appearance of a new peak at 445 nm ($\epsilon = 2000 \text{ M}^{-1} \text{ cm}^{-1}$) (Figure 2a). The yellowish orange species **1**, which was metastable at 25 °C ($t_{1/2} \sim 1 \text{ h}$), was characterized by various spectroscopic methods. The electrospray ionization mass spectrum (ESI-MS) of **1** exhibited prominent mass peaks at $m/z = 254.6$ and 608.0 , whose mass and isotope distribution patterns correspond to $[\text{Ru}^{\text{IV}}(\text{O})(\text{terpy})(\text{bpm})]^{2+}$ (calc. $m/z = 254.5$) and $[\text{Ru}^{\text{IV}}(\text{O})(\text{terpy})(\text{bpm})(\text{ClO}_4)]^+$ (calc. $m/z = 608.0$), respectively (Figure 2b). When **1** was generated with isotopically labeled PhI^{18}O , the mass peak at $m/z = 608.0$ due to $1\text{-}^{16}\text{O}$ shifted to $m/z = 610.0$ due to $1\text{-}^{18}\text{O}$, indicating that **1** contains one oxygen atom. The resonance Raman (rRaman) spectrum of **1** exhibited a vibration at 798 cm^{-1} , which shifted to 757 cm^{-1} upon introduction of ^{18}O (Figure 2c). The observed isotopic shift of $\Delta\nu = 41 \text{ cm}^{-1}$ upon ^{18}O -substitution is in a good agreement with the calculated value of $\Delta\nu = 41 \text{ cm}^{-1}$ for the Ru-O diatomic vibration, as reported for other $\text{Ru}(\text{IV})\text{-oxo}$ species.^{19,43,45} It is also in agreement with our DFT calculated Ru-O vibration frequency, which was found to be at 796 cm^{-1} and shifted to 758 cm^{-1} upon ^{18}O substitution. The X-band electron paramagnetic resonance (EPR) spectrum of **1** was silent, consistent with **1** being an integer spin system. The spin state of **1** was then determined using ^1H NMR technique of Evans;^{61,62} a magnetic moment of 3.3 B.M. at $-20 \text{ }^\circ\text{C}$ indicates that **1** is an intermediate-spin ($S = 1$) $\text{Ru}^{\text{IV}}(\text{O})$ complex (see Experimental Section; see also Supporting Information (SI), Figure S1 for ^1H NMR spectrum of **1**). DFT calculations confirmed that the lowest spin state was the $S = 1$ state, 14.1 and 60.3 kcal mol^{-1} (in Gibb's free energy, ΔG) lower than the $S = 0$ and $S = 2$ states, respectively (SI, Table S1). The high energy of the $S = 2$ state is due to high lying σ_{xy}^* and $\sigma_{z,2}^*$ orbitals, effectively ruling out any reactions associated with participation of these orbitals. Taken together, the spectroscopic and computational data clearly demonstrate that **1** is an $S = 1$ $[\text{Ru}^{\text{IV}}(\text{O})(\text{terpy})(\text{bpm})]^{2+}$ complex (Figure 1).

C-H Bond Activation Reaction by 1. We carried out the C-H bond activation reactions using substrates with bond

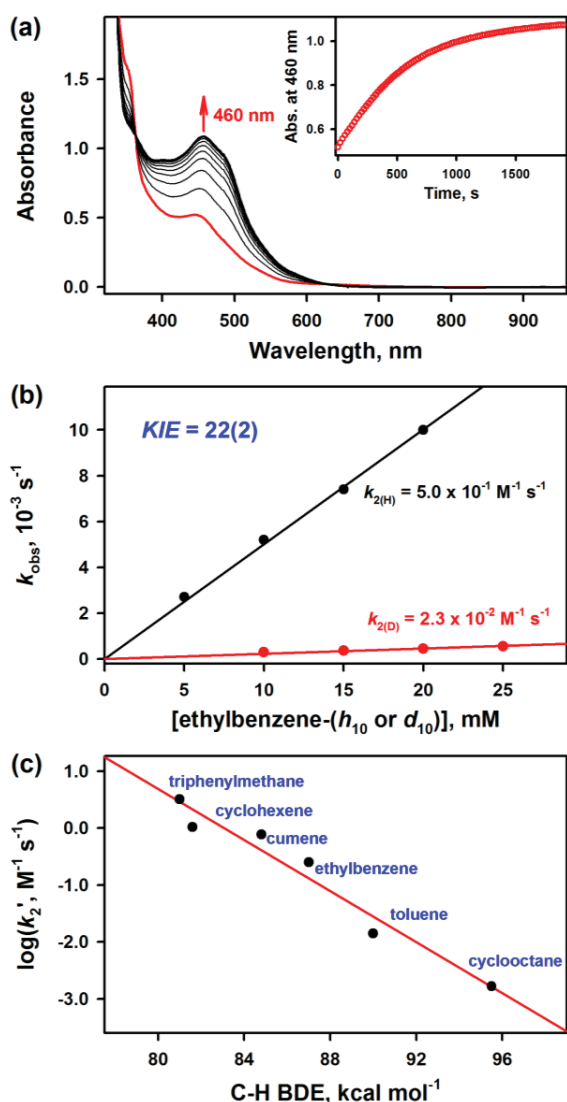


Figure 3. (a) UV-vis spectral changes observed in the reaction of **1** (0.25 mM, red line) and ethylbenzene (5.0 mM) in CH_3CN at 25 °C. Inset shows the time course monitored at 460 nm. (b) Plots of pseudo-first-order rate constants, k_{obs} (s^{-1}), against concentrations of ethylbenzene- h_{10} (black circles) and ethylbenzene- d_{10} (red circles) to determine second-order rate constants (k_2) in CH_3CN at 25 °C. (c) Plot of $\log k_2'$ versus C-H BDEs of substrates. The k_2' values are obtained by dividing second-order rate constants (k_2) by the number of

dissociation energies (BDEs) between 81.0 kcal mol⁻¹ (triphenylmethane) and 95.5 kcal mol⁻¹ (cyclooctane) in CH_3CN at 25 °C. Upon addition of ethylbenzene to the solution of **1**, the UV-vis peak at 445 nm was slowly converted to a new peak at 460 nm with clean isobestic points at 337, 363, and 628 nm (Figure 3a). The first-order rate constants (k_{obs}), determined by pseudo-first-order fitting of the kinetic data for the formation at 460 nm, increased proportionally with the increase of ethylbenzene concentration, leading us to determine a

second-order rate constant (k_2) of $5.0 \times 10^{-1} \text{ M}^{-1} \text{ s}^{-1}$ (Figure 3b). Similarly, when we used deuterated ethylbenzene- d_{10} as a substrate, a second-order rate constant (k_2) of $2.3 \times 10^{-2} \text{ M}^{-1} \text{ s}^{-1}$ was obtained. Thus, a kinetic isotope effect (KIE) value of 22(2) was obtained in the oxidation of ethylbenzene versus ethylbenzene- d_{10} in CH_3CN at 25 °C (Figure 3b). Second order rate constants for other alkanes were determined similarly (SI, Figure S2), and Figure 3c shows a good linear correlation between the logarithm of k_2' and the C-H BDEs of the substrates. On the basis of the large KIE value and the good correlation between the logarithms of k_2' and the substrate BDE values, we conclude that the C-H bond activation of alkanes by **1** occurs via a H-atom abstraction from substrate C-H bonds as the rate-determining step (r.d.s.) (Scheme 1A, pathway a).^{32,35}

Product analysis of the reaction solution of **1** and ethylbenzene revealed the formations of 1-phenylethanol (27(4)%), acetophenone (8(3)%), and styrene (2(1)%) under Ar atmosphere. The total product yield of 45%, calculated accounting for the fact that acetophenone is a 4- e^- oxidation product, suggests that one molecule of substrate was oxidized by two molecules of $\text{Ru}^{\text{IV}}\text{O}$ (vide infra). When the ethylbenzene oxidation was performed by $1\text{-}^{18}\text{O}$, the 1-phenylethanol product was found to contain 71(5)% of ^{18}O (SI, Figure S3), demonstrating that the source of oxygen in the 1-phenylethanol product was $1\text{-}^{18}\text{O}$. When the reaction was carried out in the presence of air, the yields of 1-phenylethanol, acetophenone, and styrene were 16(4), 30(3), and 8(3)%, respectively. In addition, when the oxidation reaction of ethylbenzene by **1** was performed in the presence of CCl_3Br (500 equiv) under Ar atmosphere, 1-bromoethylbenzene was obtained as the sole product.⁵⁴

We also characterized the Ru product formed in the reaction of **1** and ethylbenzene by EPR and ESI-MS. The X-band EPR spectrum of the Ru product showed signals with $g = 2.42$, $g = 2.16$, and $g = 1.91$, indicating the oxidation state of +3 for the Ru product (SI, Figure S4a).⁴⁵ The ESI-MS of the solution exhibited a prominent mass peak at $m/z = 255.1$, whose mass and isotope distribution pattern correspond to $[\text{Ru}^{\text{III}}(\text{terpy})(\text{bpm})(\text{OH})]^+$ (calc. $m/z = 255.0$) (SI, Figure S4b). Further, addition of 1 equiv of 1,1'-dimethylferrocene (Me_2Fc) to the complete reaction solution of **1** and ethylbenzene resulted in the formation of Ru^{II} and 1,1'-dimethylferrocenium ion (Me_2Fc^+) with >90% yield (SI, Figure S5a), indicating that the Ru^{III} species produced was reduced to Ru^{II} by Me_2Fc (see also SI, Figure S5b for ESI-MS). Thus, all the results discussed above strongly support that $\text{Ru}^{\text{III}}\text{-OH}$ species, not Ru^{II} species, was formed in the reaction of ethylbenzene by **1**.

The observations described above are contrary to the oxygen rebound mechanism, since the hydroxylation of alkanes by $\text{Ru}^{\text{IV}}\text{O}$ species should yield Ru^{II} species as a 2 e^- reduced product in the oxygen rebound mechanism.^{34,35,45} Since we could not rule out a possibility that the Ru^{III} formation resulted from comproportionation of $\text{Ru}^{\text{IV}}(\text{O})$

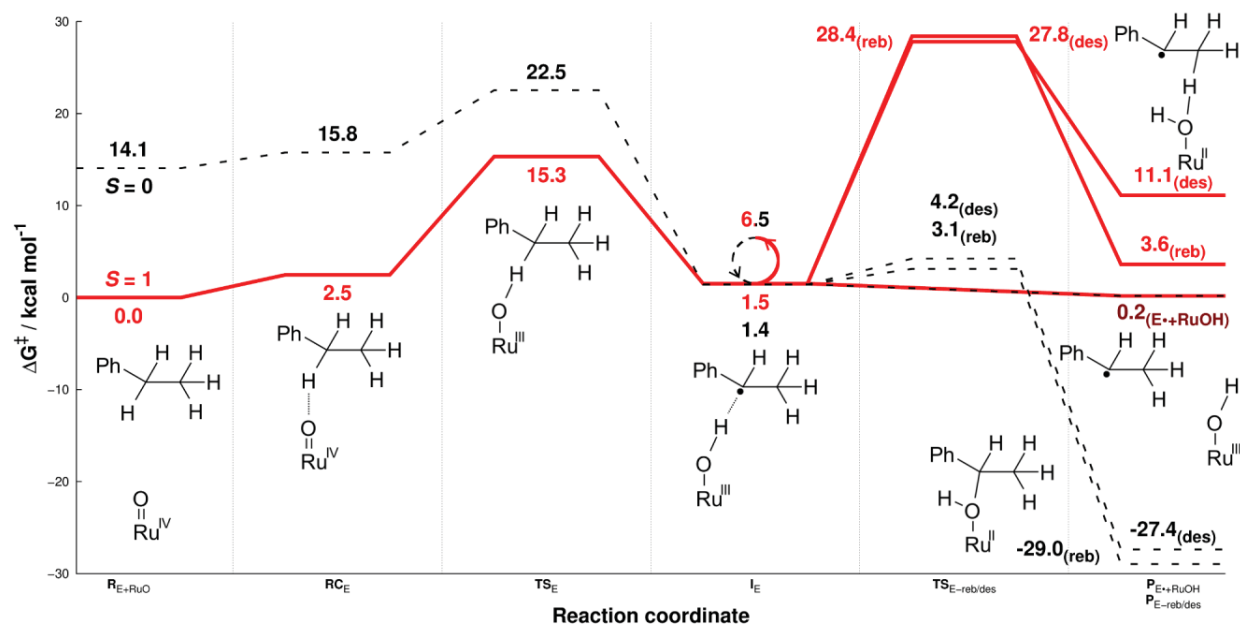


Figure 4. Reaction energy profile of the ethylbenzene C-H activation reaction by **1** at 25 °C. The initial HAT reaction in the $S = 1$ state creates a substrate intermediate 3I_E , where the reaction has a number of choices (see text), including spin flipping (marked with a loop in the center of the graph) with an estimated minimum energy barrier of 5.0 kcal mol⁻¹. The lowest energy pathway is therefore the $S = 1$ dissociation pathway where the product state (${}^3P_{E+RuOH}$) is only 0.20 kcal mol⁻¹ above the separated reactants, ${}^3R_{E+RuO}$.

and Ru^{II} species, we carried out a control reaction by reacting equal amounts of **1** and [Ru^{II}(terpy)(bpm)]²⁺. In this reaction, no formation of Ru^{III} species was observed in UV-vis, EPR, and ESI-MS (SI, Figure S6), leading us to conclude that the Ru^{III}-OH species was formed exclusively from the H-atom abstraction reaction of alkanes by **1**, but not from the comproportionation of Ru^{IV}(O) and Ru^{II} species.

Then, how is the Ru^{III}-OH species formed in the C-H bond activation of alkanes by **1**? We propose that after Ru^{III}-OH and alkyl radical species are formed in the first step of the C-H bond activation by **1** (Scheme 1A, pathway a), the dissociation process is the preferred pathway (Scheme 1A, pathway e), rather than the oxygen rebound (Scheme 1A, pathways b and c) and desaturation (Scheme 1A, pathway d) processes. This conclusion is reached based on the results of the organic products formed in the presence of O₂ (i.e., the substrate radical dissociation from Ru^{III}OH and reaction with O₂ to give hydroxylated products) and in the presence of CCl₃Br (i.e., the substrate radical dissociation from Ru^{III}OH and reaction with CCl₃Br to give brominated product) as well as the presence of the Ru^{III} product. These results are in line with our earlier results reported in the reactions of nonheme Fe^{IV}O, Mn^{IV}O, Cr^{IV}O, and Fe^VO complexes.⁵⁴⁻⁵⁹

To support the dissociation hypothesis, we performed DFT calculations for the reaction of **1** and ethylbenzene (SI, Tables S2, S7, and S12). The DFT calculations resulted in a reaction barrier of 15.3 kcal mol⁻¹ for the $S = 1$ state (3TS_E , Figure 4, the left superscript refers to the

multiplicity $M = 2S + 1$ per convention), relative to the sum of the energies of the separated reactants (${}^3R_{E+RuO}$, as opposed to the reactant complex, 3RC_E). This step was found to be the r.d.s. (Scheme 1A, pathway a), comparable to the experimentally determined barrier of 18.3 kcal mol⁻¹ (obtained by converting k_2' through the Eyring equation). A two-spin state reaction was ruled out at this step of the reaction as the $S = 0$ state 1TS_E was high in energy (22.5 kcal mol⁻¹). Hence, after the initial H-atom abstraction step, the resulting Ru^{III}OH species is in $S = 1/2$ state, while the substrate has an α -radical, in total making it an $S = 1$ state (3I_E). In the second step, the reaction has four pathway choices; *i*) the rebound reaction (Scheme 1A, pathways b and c), *ii*) abstracting another H-atom from the substrate to perform a desaturation reaction (Scheme 1A, pathway d), *iii*) dissociating (Scheme 1A, pathway e), or *iv*) changing the α -spin of the substrate to a β -spin and performing the rebound/desaturation/dissociation reaction on the $S = 0$ spin state surface. The first two choices (*i* and *ii*) are ruled out as their transition states, ${}^3TS_{E-reb}$ and ${}^3TS_{E-des}$, were found to be at 28.4 and 27.8 kcal mol⁻¹ above the reactants, respectively. The dissociation option (*iii*) is then much more preferable with an exothermic dissociation energy of 1.3 kcal mol⁻¹ (i.e., the dissociated products ${}^3P_{E+RuOH}$ are 0.20 kcal mol⁻¹ above ${}^3R_{E+RuO}$).

The spin flip option (*iv*) to reach 1I_E is in principle possible. As the $S = 0$ rebound (${}^1TS_{E-reb}$) and desaturation (${}^1TS_{E-des}$) transition states are very low (3.1 and 4.2 kcal mol⁻¹, respectively) and the spin orbit coupling on Ru is

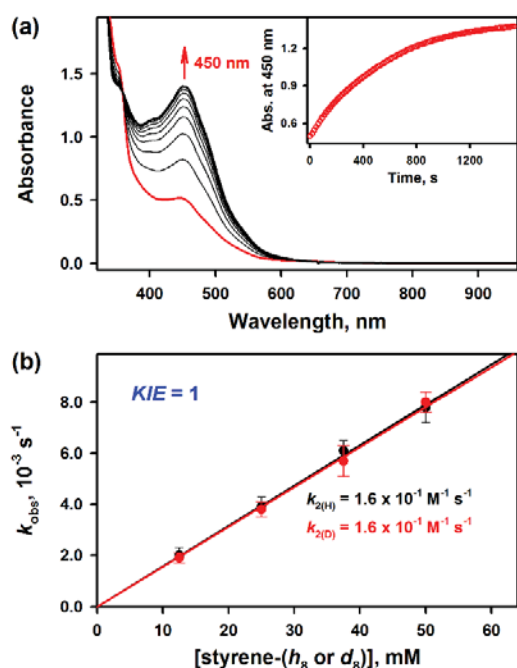


Figure 5. (a) UV-vis spectral changes observed in the reaction of **1** (0.25 mM, red line) and styrene (13 mM) in CH₃CN at 25 °C. Inset shows the time course monitored at 450 nm. (b) Plots of pseudo-first-order rate constants, k_{obs} (s⁻¹), against concentrations of styrene-*h*₈ (black circles) and styrene-*d*₈ (red circles) to determine second-order rate constants, k_2 , and KIE value in CH₃CN at 25 °C.

large, this pathway would seem to be competitive with the $S = 1$ dissociation reaction. However, a spontaneous spin flip of a carbon-centered radical is not necessarily an ultra-fast process. We have previously argued that, even if we assume an ultra-fast spin flip process of 10^9 s⁻¹, this would still be equivalent to having an energy barrier of 5.0 kcal mol⁻¹ according to the Eyring equation at room temperature.⁵⁶ This would not be competitive with the dissociation energy of 1.3 kcal mol⁻¹. Even if the spin flip occurs, however, the dissociation energy at the $S = 0$ state is still exothermic by 1.2 kcal mol⁻¹. Hence, the dissociation mechanism will likely be preferred anyhow, which is more in line with our experimental results showing 45% yield of products compared to the projected 50% product yield in the dissociative mechanism.⁵⁴⁻⁵⁹

An additional issue in this reaction is the tunneling, as indicated by the high experimental KIE. Using Eckart tunneling,⁶³ we found that tunneling effect corresponds to lowering the $S = 1$ ethylbenzene-*h*₁₀ and -*d*₁₀ barriers by 1.8

kcal mol⁻¹ and 1.0 kcal mol⁻¹, respectively (Table S2). Without these effects, the KIE value would have been 7, using the free energies. With tunneling, the KIE value is now 25, which is close to the experimental value of 22(2).

Epoxidation of Styrene by 1. We investigated the olefin oxidation using styrene-*h*₈ and styrene-*d*₈ as substrates. Upon addition of styrene to the solution of **1** in CH₃CN at 25 °C, **1** decayed with the formation of a new peak at 450 nm (Figure 5a). The first-order rate constants (k_{obs}), determined by pseudo-first-order fitting of the kinetic data at 450 nm, increased proportionally with the increase of substrate concentrations, affording the second-order rate constants of 1.6×10^{-1} M⁻¹ s⁻¹ for both the reactions of styrene and styrene-*d*₈ (Figure 5b). The KIE value of **1** suggests that the reaction of **1** with the olefins does not occur via an H-atom abstraction pathway, but via an OAT to the C=C double bond (Scheme 1C). Indeed, styrene oxide (84(5)%) was formed as the major product with the formation of a small amount of 2-phenylacetaldehyde (4(1)%) under Ar atmosphere. In the reaction where **1**-¹⁸O was used, the styrene oxide product contained 78(4)% of ¹⁸O (SI, Figure S9), suggesting that the oxygen in the styrene oxide product derived from the Ru^{IV}O species. The characterization of the Ru product formed in the epoxidation reaction was also carried out using EPR and ESI-MS. The EPR spectrum was silent, suggesting the formation of Ru^{II} species as the end product. The ESI-MS data exhibited mass peaks corresponding to [Ru^{II}(terpy)(bpm)(CH₃CN)]²⁺ (SI, Figure S7; also see SI, Figure S8 for the conversion of the peak at 485 nm due to [Ru^{IV}(terpy)(bpm)(H₂O)]²⁺ to the peak at 450 nm due to [Ru^{II}(terpy)(bpm)(CH₃CN)]²⁺). Based on the product analysis of the reaction solution of **1** and styrene, we conclude that styrene was oxidized to styrene oxide with the conversion of **1** to Ru^{II} species (Scheme 1C).

DFT calculations (SI, Tables S3, S8, and S13) reveal that, in the $S = 1$ state, this reaction would have been a two-step process (Figure 6). In the first step, **1** attacks the terminal C-atom to form a Ru-O-C bonded intermediate ³I_S, over a transition state at 14.4 kcal mol⁻¹ (³TS_{1S}). The alternative of attacking the other C-atom in the ethane group has a higher transition state at 22.8 kcal mol⁻¹ (not shown). The second step involves closing the epoxide ring. However, it is found that this step goes over a transition state ³TS_{2S} at 31.6 kcal mol⁻¹, to a Ru^{II} product that is at 22.4 kcal mol⁻¹ (³P_S). Hence, with the high barrier and an endothermic reaction energy, the reaction at the $S = 1$ surface seems less probable.

In the $S = 0$ state, the epoxidation reaction features a one-step process over a single transition state ${}^1\text{TS}_S$ at 22.6 kcal mol⁻¹. This energy barrier is on the high side, especially compared to ${}^3\text{TS}_{1S}$ (14.4 kcal mol⁻¹) and also the experimental value (k_2 corresponding to 18.5 kcal mol⁻¹), but it is lower than ${}^3\text{TS}_{2S}$ (31.6 kcal mol⁻¹). Moreover, the Ru^{II} product ${}^1\text{P}_S$ is 34.5 kcal mol⁻¹ more preferred than ${}^3\text{P}_S$. It is, in fact, a well known experimental fact that Ru^{II} is an $S = 0$ species. Thus, it is clear that a spin state flip to $S = 0$ has to occur somewhere along the reaction pathway. Based on our calculated data, we propose that this occurs at ${}^3\text{I}_S$. In this way, the reaction can utilize the low ${}^3\text{TS}_{1S}$ to perform half of the reaction. Then, a spin flip will allow the reaction to bypass the high ${}^3\text{TS}_{2S}$, and close the epoxide ring. Indeed, we found a minimum energy crossing point (MECP) between these two states at 2.5 kcal mol⁻¹ in electronic energy (ΔE), where optimization from this geometry with $S = 1$ led to ${}^3\text{I}_S$, and with $S = 0$ to ${}^1\text{P}_S$. While we cannot calculate the final ΔG for the MECP (which would be dependent on, among other things, thermal contributions and spin inversion probabilities), assuming that the corrections to the electronic energy is less than 10 kcal mol⁻¹, the rate-limiting barrier is ${}^3\text{TS}_{1S}$.

C-H Bond Activation versus Epoxidation in the Oxidation of Cyclohexene by **1.** We then investigated the reaction of **1** with cyclohexene-*h*₁₀ and cyclohexene-*d*₁₀ in CH₃CN at 25 °C. Upon addition of cyclohexene to the solution of **1**, we observed the formation of a new peak at 460 nm (SI, Figure S10); the spectral change was similar to that observed in the C-H bond activation of ethylbenzene by **1** (Figure 3a). A second-order rate constant of $k_2 = 4.2(4) \text{ M}^{-1} \text{ s}^{-1}$ was determined, and a k_2' value was obtained by dividing the second-order rate constant (k_2) with the number of equivalent target C-H bonds in cyclohexene (e.g., $k_2' = k_2/4$). The log k_2' of this reaction fits well into the line in Figure 3c, implying that the oxidation of cyclohexene by **1** occurs via a C-H bond activation process. When cyclohexene-*d*₁₀ was used as a substrate, $k_2 = 1.1(1) \times 10^{-1} \text{ M}^{-1} \text{ s}^{-1}$ was obtained, thus giving a large KIE

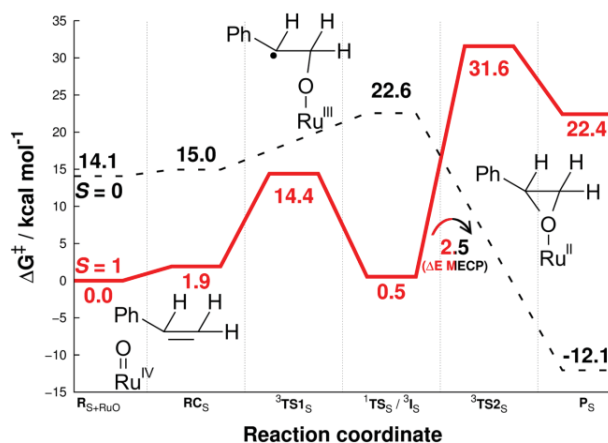


Figure 6. Reaction energy profile of the styrene epoxidation by **1** at 25 °C. The $S = 1$ surface features a two-step reaction mechanism, whereas the $S = 0$ surface shows a concerted one-step mechanism. A change in spin state is proposed after the ${}^3\text{I}_S$ step, marked with an arrow.

value of 38(3) (Figure 7).^{32,34} Further, activation parameters, enthalpy (ΔH^\ddagger) and entropy (ΔS^\ddagger), determined in the reactions of **1** with cyclohexene-*h*₁₀ and cyclohexene-*d*₁₀ were different depending on the substrates (SI, Figure S11a), whereas the reactions of **1** with styrene-*h*₈ and styrene-*d*₈ showed that the enthalpy and entropy values were the same irrespective of the substrates (i.e., styrene and deuterated styrene; SI, Figure S11b). The results regarding KIE and activation parameters indicate that the oxidation of cyclohexene by **1** occurs via a C-H bond activation reaction including tunneling. Based on observations of the good BDE correlation with log k_2' (Figure 3c) and the large KIE value (Figure 7), we conclude that an H-atom abstraction in the allylic α -C-H bond activation of cyclohexene by **1** is the r.d.s. (Scheme 1B, pathway *g*), which is different from the C=C double bond epoxidation of styrene (Scheme 1C).

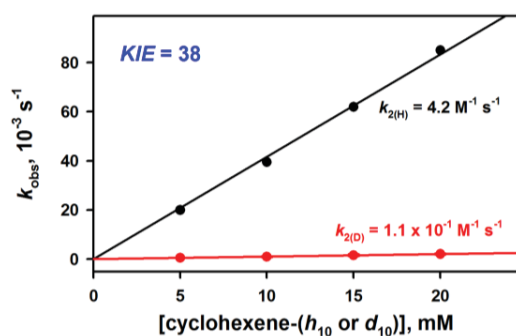


Figure 7. Plots of the pseudo-first-order rate constants, k_{obs} (s^{-1}), against concentrations of cyclohexene- h_{10} (black circles) and cyclohexene- d_{10} (red circles) to determine second-order

When we carried out product analysis in the cyclohexene oxidation by **1** under Ar atmosphere, 26(3)% of cyclohex-2-enol and 8(2)% of cyclohex-2-enone, in total 42% (26 + 8 × 2%) yield, were obtained as products (Table 1). No formation of cyclohexene oxide product was observed in this reaction. Cyclohex-2-enol formed in the cyclohexene oxidation by **1**- ^{18}O contained 82(4)% of ^{18}O (SI, Figure S12), showing that the source of oxygen in the product was **1**. The decayed Ru product in the reaction of **1** and cyclohexene was determined to be $\text{Ru}^{\text{III}}\text{-OH}$ species by analyzing the reaction solution with ESI-MS and EPR spectroscopies and by carrying out a reaction with Me_2Fc ; the Ru product was the same as that obtained in the ethylbenzene oxidation by **1** (SI, Figures S4 – S6). Interestingly, when we used cyclohexene- d_{10} , a small amount of cyclohexene oxide (7(2)%) was obtained along with cyclohex-2-enol (21(2)%) and cyclohex-2-enone (9(3)%).⁵⁹ Taken altogether, the experimental results demonstrate that a H-atom abstraction by **1** is the r.d.s. (Scheme 1B, pathway *g*) and the oxygen non-rebound mechanism takes place (Scheme 1B, pathways *j* and *k*); the reaction mechanism is identical to that proposed in the oxidation of ethylbenzene by **1**.

DFT calculations (SI, Tables S4, S9, and S14) show that the H-atom abstraction of cyclohexene is the r.d.s. with.

Table 1. Oxidation Products of Cyclohexene- h_{10} and Cyclohexene- d_{10} by **1**^a

substrate	product	yield (%)
cyclohexene- h_{10}	cyclohex-2-enol	26(3)
	cyclohex-2-enone	8(2)
	cyclohexene oxide	trace
cyclohexene- d_{10}	cyclohex-2-enol	21(2)
	cyclohex-2-enone	9(3)
	cyclohexene oxide	7(2)

^a Reaction conditions: Reactions were run with **1** (1.0 mM) and substrates (50 mM) under Ar atmosphere in CH₃CN at 25 °C. See experimental section for product

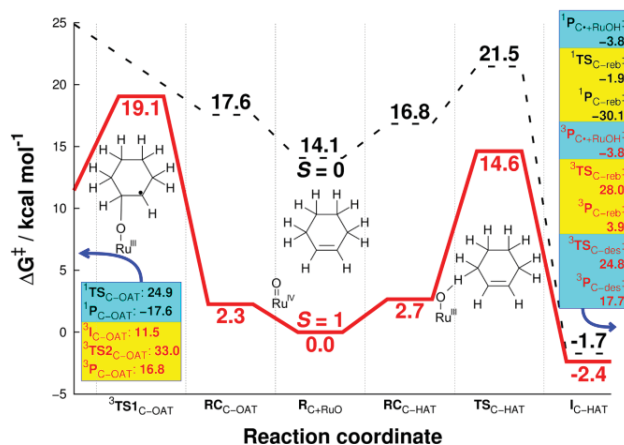


Figure 8. Epoxidation versus C-H bond activation reaction energy profile for the cyclohexene oxidation reactions by **1** at 25 °C, showing only the first steps of the reactions. Starting from the middle of the graph, the C-H bond activation reaction goes in the right direction over a minimum barrier of 14.6 kcal mol⁻¹. Epoxidation, going to the left, has a higher minimum barrier of 19.1 kcal mol⁻¹. The entire shape of the potential energy surface is similar to those for ethylbenzene for C-H bond activation (Figure 4) and styrene for epoxidation (Figure 4). The oxygen non-rebound pathway is here indeed preferred as well, with energies at -3.85 / 28.0 / 24.8 kcal mol⁻¹ (³ $\text{P}_{\text{C}^+-\text{RuOH}}$ / ³ $\text{TS}_{\text{C-reb}}$ / ³ $\text{TS}_{\text{C-des}}$, respectively). Again, the $S = 0$ second step barriers are low, but the same arguments against spin inversion here apply as in the ethylbenzene case (vide supra). Likewise, the energetic profile of cyclohexene epoxidation is similar to the styrene epoxidation described above. The $S = 1$ epoxidation occurs in a two-step process, whereas the $S = 0$ surface contains one TS (³ $\text{TS}_{\text{C-OAT}}$ / ¹ $\text{TS}_{\text{C-OAT}}$ / ³ $\text{TS}_{\text{C-OAT}}$ at 19.1 / 33.0 / 24.9 kcal mol⁻¹, respectively). Thus, spin inversion likely occurs here at ³ $\text{I}_{\text{C-OAT}}$ as well. However, since ³ $\text{TS}_{\text{C-OAT}}$ (19.1 kcal mol⁻¹) is 4.5 kcal mol⁻¹ higher than ³ $\text{TS}_{\text{C-HAT}}$ (14.6 kcal mol⁻¹), the H-atom abstraction reaction takes precedence over the OAT reaction, in agreement with experiments. Upon deuteration, this difference is reduced to 2.6 kcal mol⁻¹, making partial epoxidation possible. The KIE values here are again more in agreement with the experimental value of 38 when including tunneling effects (using Eckart tunneling: KIE = 24), compared to without tunneling (KIE = 6).

Sulfoxidation by 1. Finally, we investigated the oxidation of sulfides by **1**. Upon addition of thioanisole to the CH₃CN solution of **1** at -40 °C, the intermediate decayed with the appearance of a peak at 485 nm (SI, Figure S13). The pseudo-first-order rate constant increased linearly with the increase of thioanisole concentration to give a second-order rate constant of $k_2 = 3.1(4) \text{ M}^{-1} \text{ s}^{-1}$ (Figure 9a). When *para*-X-substituted thioanisoles (X = OMe, Me, H, Br, and CN) were used in the sulfoxidation reaction, a ρ

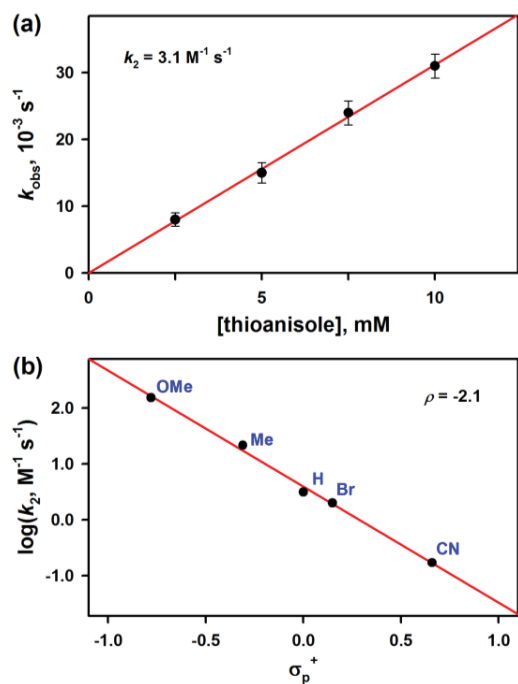


Figure 9. (a) Plot of pseudo-first-order rate constants, k_{obs} (s^{-1}), against thioanisole concentration to determine a second-order rate constant in the reaction of **1** and thioanisole in CH_3CN at -40°C . (b) Hammett plot of $\log k_2$ against σ_p^+ of *para*-X-substituted thioanisole derivatives ($X = \text{OMe}, \text{Me}, \text{H}, \text{Br}$, value of -2.1 was obtained from the Hammett plot of $\log k_2$ against σ_p^+ (Figure 9b; SI, Figure S14). This result indicates that the Ru-oxo group of **1** possesses an electrophilic character. In addition, when the rate constants were plotted against the oxidation potential (E_{ox}) of thioanisole derivatives, we observed a good linear correlation with a slope of -6.1 (SI, Figure S15), suggesting that the oxidation of thioanisoles by **1** occurs via a direct OAT mechanism (Scheme 1C, pathway *m*), as proposed in the oxidation of PPh_3 or PET_3 by other $\text{Ru}^{\text{IV}}\text{O}$ species.^{48,64}

Product analysis of the reaction solution revealed that methyl phenyl sulfoxide was formed as a sole product (85(5)% yield based on the amount of **1** used). When the thioanisole oxidation was performed by $\text{1-}^{18}\text{O}$, the methyl phenyl sulfoxide product contained 70(5)% of ^{18}O , indicating that the source of the oxygen atom in the sulfoxide product was **1** (SI, Figure S16a). Based on the analysis of the reaction solution using EPR (not shown, but a silent EPR spectrum) and ESI-MS (SI, Figure S16b), we found that a Ru^{II} species was formed as the decayed product of **1** in this reaction.

As shown in Figure 10, DFT calculations (SI, Tables S5, S10, and S15) show a single-step reaction with $^3\text{TS}_\text{T}$ at 18.7 kcal mol^{-1} (at -40°C). Interestingly, $^1\text{TS}_\text{T}$ was lower in energy at 14.6 kcal mol^{-1} , a contributing factor to this being the lower energy of the $S = 0$ Ru^{II} product. Given the very low experimentally determined energy barrier (13.0 kcal mol^{-1}), we propose that two-spin state reactivity

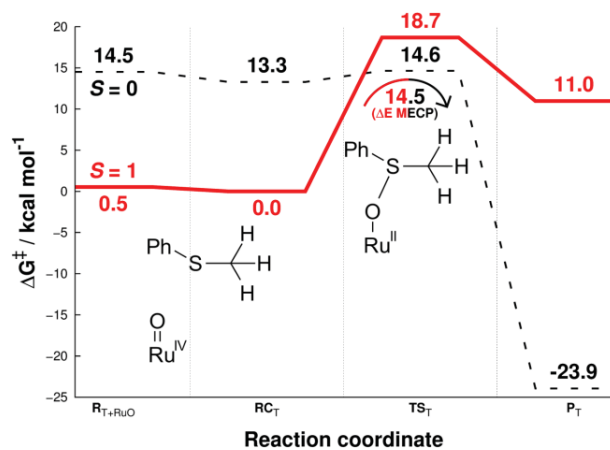


Figure 10. Reaction energy profile for the sulfoxidation reaction of thioanisole by **1** at -40°C . A spin state change is predicted to occur near $^1\text{TS}_\text{T}$ so that the low energy $^1\text{TS}_\text{T}$ can be utilized, which is consistent with the fast experimental rates observed in this reaction.

is in play here, where the reaction switches to the $S = 0$ surface to utilize the low-lying $^1\text{TS}_\text{T}$. In fact, an MECP was found just after $^1\text{TS}_\text{T}$ at $\Delta E = 14.5$ kcal mol^{-1} , where geometry optimization on one side resulted in $^3\text{RC}_\text{T}$ and on the other side in $^1\text{P}_\text{T}$.

CONCLUSION

In summary, the C-H bond activation, epoxidation, and sulfoxidation reactions by mononuclear nonheme $\text{Ru}^{\text{IV}}\text{O}$ complexes have been investigated over the past three decades;²⁴⁻⁴⁸ however, some of the proposed mechanisms in the oxidation reactions are still controversial and remain elusive, especially in the C-H bond activation reactions of alkanes and olefins containing allylic C-H bonds. Moreover, we have shown recently that mononuclear nonheme metal-oxo complexes conduct the C-H bond activation reactions via an oxygen non-rebound mechanism, not via a conventional oxygen rebound mechanism.⁵⁴⁻⁵⁹ We therefore reinvestigated the mechanisms of the alkane hydroxylation, C-H bond activation versus olefin epoxidation in cyclohexene oxidation, and oxygen atom transfer reactions with a spectroscopically well-characterized $\text{Ru}^{\text{IV}}\text{O}$ complex, $[\text{Ru}^{\text{IV}}(\text{O})(\text{terpy})(\text{bpm})]^{2+}$, using both experimental and theoretical methods. In the alkane hydroxylation, both the experimental and theoretical results demonstrate unambiguously that the dissociation of the substrate radical formed via a rate-determining H-atom abstraction of alkane C-H bonds is more favorable than the oxygen rebound and desaturation processes. In the oxidation of olefins containing allylic C-H bonds, the experimental results show the preference on the H-atom abstraction over the C=C double bond epoxidation in the oxidation of cyclohexene by **1** and are further supported by DFT calculations, in which the energy barrier for the C-H activation barrier is indeed lower than the epoxidation energy barrier. In contrast, olefins without the allylic C-H

bonds are oxidized to give epoxide products via an OAT mechanism. In sulfoxidation reaction, it is shown that **1** possesses an electrophilic character and conducts the sulfoxidation via an OAT mechanism. DFT calculations propose that two-spin state reactivity is in play in both the epoxidation and sulfoxidation reactions. Taken together, the present work adds one more piece of evidence that the C-H bond activation of alkanes by a mononuclear nonheme Ru^{IV}O complex occurs via an oxygen non-rebound mechanism, as we have shown in the reactions of mononuclear nonheme Fe^{IV}O, Mn^{IV}O, Cr^{IV}O, and Fe^VO complexes.⁵⁴⁻⁵⁸ We have also shown that the C-H bond activation is a preferred pathway over the C=C double bond epoxidation in the oxidation of cyclohexene by a mononuclear nonheme Ru^{IV}O complex, similar to the case of mononuclear nonheme Fe^{IV}O complex.⁵⁹

EXPERIMENTAL SECTION

Materials. [Ru^{II}(terpy)(bpm)(H₂O)](ClO₄)₂ and PhIO were prepared according to the literature procedure.^{60,65-67} All other chemicals were obtained from Aldrich Chemical Co. and used without further purification unless otherwise indicated. Solvents were dried according to the reported procedures and distilled under Ar prior to use.⁶⁸ H₂¹⁸O (95 % ¹⁸O-enriched) was purchased from ICON Services Inc. (Summit, NJ, USA).

Instrumentation. UV-vis spectra were recorded on a Hewlett Packard Agilent 8453 UV-visible spectrophotometer equipped with a circulating water bath or an UNISOKU cryostat system (USP-203, Japan). Electrospray ionization mass spectra (ESI-MS) were collected on a Thermo Finnigan (San Jose, CA, USA) LCQTM Advantage MAX quadrupole ion trap instrument, by infusing samples directly into the source at 20 μ L/min using a syringe pump. The spray voltage was set at 4.7 kV and the capillary temperature at 80 °C. Electron paramagnetic resonance (EPR) spectra were recorded at 5 K using X-band Bruker EMX-plus spectrometer equipped with a dual mode cavity (ER 4116DM). The low temperatures were achieved and controlled with Oxford Instruments ESR900 liquid He quartz cryostat with Oxford Instruments ITC503 temperature and gas flow controller. The experimental parameters for EPR measurements were as follows: microwave frequency = 9.646 GHz, microwave power = 1.0 mW, modulation amplitude = 10 G, gain = 1×10^4 , modulation frequency = 100 kHz, time constant = 40.96 ms and conversion time = 85.00 ms. Resonance Raman spectra were recorded using liquid nitrogen cooled CCD detector (model LN/CCD-1340 \times 400PB, Princeton Instruments) attached to a 1-m single polychromator (model MC-100DG, Ritsu Oyo Kogaku). An excitation wavelength of 406.7-nm was provided by a Kr⁺ laser (Spectra Physics, BeamLok 2060-RM), with 4.0 mW power at the samples. All measurements were carried out with a spinning cell (1000 rpm) at -20 °C. Raman shifts were calibrated with indene,

and the accuracy of the peak positions of the Raman bands was ± 1 cm⁻¹. Product analysis was performed with an Agilent Technologies 6890N gas chromatograph (GC) and Thermo Finnigan (Austin, Texas, USA) FOCUS DSO (dual stage quadrupole) mass spectrometer interfaced with Finnigan FOCUS gas chromatograph (GC-MS). ¹H NMR spectra were measured with Bruker model digital AVANCE III 400 FT-NMR spectrometer.

Generation and Characterization of **1.** The yellowish orange species **1** was generated by adding 1.2 equiv of PhIO (dissolved in MeOH) to the freshly prepared CH₃CN solution of [Ru^{II}(terpy)(bpm)(H₂O)](ClO₄)₂ (0.25 mM) at 25 °C. The ¹⁸O-labeled Ru^{IV}O complex (**1**-¹⁸O) was prepared by using PhI¹⁸O in CH₃CN at 25 °C. PhI¹⁸O was prepared by mixing PhI¹⁶O (1.0 mM) solution with H₂¹⁸O (10 μ L) and stirring for about 5 min. For the resonance Raman experiment, **1**-¹⁶O and **1**-¹⁸O were generated by adding 1.2 equiv of PhI¹⁶O and PhI¹⁸O, respectively, to the solution of [Ru^{II}(terpy)(bpm)(H₂O)](ClO₄)₂ (4.0 mM) at 0 °C.

Spin-State Measurement by ¹H NMR Spectroscopy. The spin state of **1** was determined using the modified ¹H NMR method of Evans at -20 °C.^{61,62} A WILMAD[®] coaxial insert (sealed capillary) tube containing only the blank acetonitrile-*d*₃ solvent (with 1.0% TMS) was inserted into the normal NMR tube containing the complex **1** (2.0 mM) dissolved in acetonitrile-*d*₃ (with 0.1% TMS). The chemical shift of the TMS peak in the presence of the paramagnetic metal complex was compared to that of the TMS peak in the inner NMR tube. The magnetic moment was calculated using the equation, $\mu = 0.0618(\Delta\nu T/2fM)^{1/2}$, where *f* is the oscillator frequency (MHz) of the superconducting spectrometer, *T* is the absolute temperature, *M* is the molar concentration of the metal ion, and ν is the difference in frequency (Hz) between the two reference signals.⁶² The ¹H NMR Evans method allowed us to determine magnetic moment of 3.3 μ_B for **1** in CH₃CN at -20 °C, indicating that **1** possesses an *S* = 1 spin state in CH₃CN solution.

Kinetic Measurements. All reactions were run in a 1-cm UV quartz cuvette and followed by monitoring UV-Vis spectral changes of reaction solutions. Rate constants were determined under pseudo-first-order conditions (e.g., [substrate]/[**1**] > 10) by fitting the changes in absorbance for formation of peaks at 460 nm in the C-H activation, 450 nm in styrene reaction, and 485 nm in thioanisoles oxidation. The substrates with varying BDE values,⁶⁹ such as, triphenylmethane (81.0 kcal mol⁻¹), cumene (84.5 kcal mol⁻¹), ethylbenzene (87.0 kcal mol⁻¹), toluene (90.0 kcal mol⁻¹), and cyclooctane (95.5 kcal mol⁻¹) were used in the C-H bond activation reactions by **1** in CH₃CN at 25 °C. The kinetic isotope effect value (KIE) for the reaction of **1** and ethylbenzene was determined by comparing *k*₂ values obtained in the C-H and C-D bond activation reactions of ethylbenzene-*h*₁₀ and ethylbenzene-*d*₁₀, respectively. Similarly, the KIE values for the oxidation reactions of styrene and cyclohexene by **1** were obtained by using the *k*₂ values of styrene-*h*₈/styrene-*d*₈

and cyclohexene-*h*₁₀/cyclohexene-*d*₁₀, respectively. The reactions of **1** and thioanisoles were studied at -40 °C. The kinetic experiments were run at least in triplicate, and the data reported represent the average of these reactions. *k*₂' values were obtained by dividing second-order rate constants (*k*₂) with the number of equivalent target C-H bonds of substrates.

Product Analysis. Products formed in the reactions of **1** with ethylbenzene, styrene, cyclohexene, and thioanisole were analyzed by GC and GC-MS, and the product yields were determined by comparing the peak areas of sample products against standard curves prepared with known authentic samples using internal standard decane. The oxidation of ethylbenzene was achieved by mixing 0.10 M ethylbenzene with 1.0 mM of **1**. The ¹⁶O and ¹⁸O compositions in the oxygenated products of ethylbenzene, styrene, cyclohexene, and thioanisole were analyzed by comparing the relative abundances of *m/z* values which shifted by two-mass units on incorporation of ¹⁸O from **1**-¹⁸O with that of ¹⁶O-products. The Ru products (Ru^{II} and Ru^{III} species) in the reaction solutions of **1** with substrates were analysed using EPR and ESI-MS spectroscopies.

DFT Calculations. Density functional theory⁷⁰ (DFT) geometry optimizations and frequency calculations were done at UB3LYP/LACVP level⁷¹⁻⁷⁶ of theory (except for the S atom, which used 6-311G*) using Gaussian 09 package.⁷⁷ The free energies were evaluated at 25 °C, except for the thioanisole sulfoxidation calculations that were evaluated at -40 °C, in line with experiments. Solvent effects (acetonitrile) were included in the geometry optimizations by use of the CPCM implementation⁷⁸ in Gaussian 09. Single point energy evaluations were done at the UB3LYP/Def2-TZVPP level⁷⁹ including the solvent. For singlet energies, as spin contamination was found to be severe in some cases, corrections were carried out by means of spin projection.⁸⁰ Dispersion effects were included by evaluating its effects at the converged geometries by use of the DFT-D3 program using the Becke-Johnson damping.⁸¹ The energy reference point in each of the calculation series were the separated reactants (except for the sulfoxidation reaction), as this enabled us to obtain reasonable entropies (including dissociation entropy) in combination with reasonable dispersion values. These values were further corrected by a factor of 1.89 kcal mol⁻¹, as modeling complexation in solvent requires a correct treatment of the standard state.⁸² For the sulfoxidation reaction, the energy reference point was the reactant complex ³RC_T, as this state was lower in ΔG than the separated reactants. For the C-H activation reactions, tunneling corrections were earlier found to be essential,⁸³ and the barriers were therefore corrected using unsymmetrical Eckart's formalism⁶³ implemented in TheRate program.⁸⁴ All the energy values quoted in the text include all the above described effects (= ΔG), unless stated otherwise. Minimum energy crossing points (MECP) were found by using a shell script interface to

Gaussian.⁸⁵ However, only the geometry and the electronic energy (ΔE) were evaluated at the MECP, as thermal contributions cannot be evaluated at non-stationary points with regards to one specific spin state. As the Def2-TZVPP energies were different for the different spin states at the LACVP optimized structures of MECP, the average was taken as the MECP Def2-TZVPP value.

ASSOCIATED CONTENT

Supporting Information. Figures S1-S16, Tables S1-S15 and DFT calculated structure coordinates. This material is available free of charge via the Internet at <http://pubs.acs.org>.

AUTHOR INFORMATION

Corresponding Author

* E-mail: wvnam@ewha.ac.kr

Author Contributions

[§] These authors contributed equally to this work.

ACKNOWLEDGMENT

The authors acknowledge the NRF of Korea through CRI (NRF-2012R1A3A2048842 to W.N.), MSIP (2013R1A1A2062737 to K.-B.C.) and GRL (NRF-2010-00353 to W.N.). S.S. acknowledges the Israel Science Foundation (ISF grant 1183/12). SND thanks Goa University, Goa, India for grant of leave.

REFERENCES

- (1) Ortiz de Montellano, P. R. *Cytochrome P450: Structure, Mechanism, and Biochemistry*, 3rd ed.; Springer: Berlin, 2005.
- (2) Gunay, A.; Theopold, K. H. *Chem. Rev.* **2010**, *110*, 1060.
- (3) Huynh, M. H. V.; Meyer, T. J. *Chem. Rev.* **2007**, *107*, 5004.
- (4) Mayer, J. M.; *Acc. Chem. Res.* **1998**, *31*, 441.
- (5) Mayer, J. M.; *Acc. Chem. Res.* **2011**, *44*, 36.
- (6) Borovik, A. S.; *Chem. Soc. Rev.* **2011**, *40*, 1870
- (7) Hohenberger, J.; Ray, K.; Meyer, K. *Nat. Commun.* **2012**, *3*, 720.
- (8) Ray, K.; Heims, F.; Schwalbe, M.; Nam, W. *Curr. Opin. Chem. Biol.* **2015**, *25*, 159.
- (9) Chen, Z.; Yin, G. *Chem. Soc. Rev.* **2015**, *44*, 1083.
- (10) Fukuzumi, S. *Dalton Trans.* **2015**, *44*, 6696.
- (11) Nam, W. *Acc. Chem. Res.* **2007**, *40*, 522.
- (12) Shaik, S.; Hirao, H.; Kumar, D. *Acc. Chem. Res.* **2007**, *40*, 532.
- (13) Green, M. T. *Curr. Opin. Chem. Biol.* **2009**, *13*, 84.
- (14) De Visser, S. P.; Rohde, J.-U.; Lee, Y.-M.; Cho, J.; Nam, W. *Coord. Chem. Rev.* **2013**, *257*, 381.
- (15) Nam, W.; Lee, Y.-M.; Fukuzumi, S. *Acc. Chem. Res.* **2014**, *47*, 1146.
- (16) Ray, K.; Pfaff, F. F.; Wang, B.; Nam, W. *J. Am. Chem. Soc.* **2014**, *136*, 13942.
- (17) Pagliaro, M.; Campestrini, S.; Ciriminna, R. *Chem. Soc. Rev.* **2005**, *34*, 837.
- (18) Chan, S. L.-F.; Kan Y.-H.; Yip, K.-L.; Huang, J.-S.; Che, C.-M. *Coord. Chem. Rev.* **2011**, *255*, 899.

- (19) Ishizuka, T.; Ohzu, S.; Kojima, T. *Synlett*. **2014**, *25*, 1667.
- (20) Groves, J. T.; Quinn, R. J. *Am. Chem. Soc.* **1985**, *107*, 5790.
- (21) Liu, C.-J.; Yu, W.-Y.; Li, S.-G.; Che, C.-M. *J. Org. Chem.* **1998**, *63*, 7364.
- (22) Ogliaro, F.; de Visser, S. P.; Groves, J. T.; Shaik, S. *Angew. Chem., Int. Ed.* **2001**, *40*, 2874.
- (23) Sharma, P. K.; de Visser, S. P.; Ogliaro, F.; Shaik, S. *J. Am. Chem. Soc.* **2003**, *125*, 2291.
- (24) Thompson, M. S.; Meyer, T. J. *J. Am. Chem. Soc.* **1982**, *104*, 4106.
- (25) Thompson, M. S.; Meyer, T. J. *J. Am. Chem. Soc.* **1982**, *104*, 5070.
- (26) Takeuchi, K. J.; Thompson, M. S.; Pipes, D. W.; Meyer, T. J. *Inorg. Chem.* **1984**, *23*, 1845.
- (27) Dobson, J. C.; Seok, W. K.; Meyer, T. J. *Inorg. Chem.* **1986**, *25*, 1514.
- (28) Roecker, L.; Meyer, T. J. *J. Am. Chem. Soc.* **1987**, *109*, 746.
- (29) Seok, W. K.; Meyer, T. J. *J. Am. Chem. Soc.* **1988**, *110*, 7358.
- (30) Stultz, L. K.; Binstead, R. A.; Reynolds, M. S.; Meyer, T. J. *J. Am. Chem. Soc.* **1995**, *117*, 2520.
- (31) Trammell, S. A.; Wimbish, J. C.; Odobel, F.; Gallagher, L. A.; Narula, P. M.; Meyer, T. J. *J. Am. Chem. Soc.* **1998**, *120*, 13248.
- (32) Stultz, L. K.; Huynh, M. H. V.; Binstead, R. A.; Curry, M.; Meyer, T. J. *J. Am. Chem. Soc.* **2000**, *122*, 5984.
- (33) Meyer, T. J.; Huynh, M. H. V. *Inorg. Chem.* **2003**, *42*, 8140.
- (34) Bryant, J. R.; Mayer, J. M. *J. Am. Chem. Soc.* **2003**, *125*, 10351.
- (35) Bryant, J. R.; Matsuo, T.; Mayer, J. M. *Inorg. Chem.* **2004**, *43*, 1587.
- (36) Matsuo, T.; Mayer, J. M. *Inorg. Chem.* **2005**, *44*, 2150.
- (37) Che, C.-M.; Cheng, K.-W.; Chan, M. C. W.; Lau, T.-C.; Mak, C.-K. *J. Org. Chem.* **2000**, *65*, 7996.
- (38) Che, C.-M.; Yu, W.-Y.; Chan, P.-M.; Cheng, W.-C.; Peng, S.-M.; Lau, K.-C.; Li, W.-K. *J. Am. Chem. Soc.* **2000**, *122*, 11380.
- (39) Yip, W.-P.; Yu, W.-Y.; Zhu, N.; Che, C.-M. *J. Am. Chem. Soc.* **2005**, *127*, 14239.
- (40) Yip, W.-P.; Ho, C.-M.; Zhu, N.; Lau, T.-C.; Che, C.-M. *Chem. Asian J.* **2008**, *3*, 70.
- (41) Lam, W. W. Y.; Man, W.-L.; Lau, T.-C. *Coord. Chem. Rev.* **2007**, *251*, 2238.
- (42) Lam, W. W. Y.; Man, W.-L.; Leung, C.-F.; Wong, C.-Y., Lau, T.-C. *J. Am. Chem. Soc.* **2007**, *129*, 13646.
- (43) Hirai, Y.; Kojima, T.; Mizutani, Y.; Shiota, Y.; Yoshizawa, K.; Fukuzumi, S. *Angew. Chem., Int. Ed.* **2008**, *47*, 5772.
- (44) Kojima, T.; Hirai, Y.; Ishizuka, T.; Shiota, Y.; Yoshizawa, K.; Ikemura, K.; Ogura, T.; Fukuzumi, S. *Angew. Chem., Int. Ed.* **2010**, *49*, 8449.
- (45) Kojima, T.; Nakayama, K.; Ikemura, K.; Ogura, T.; Fukuzumi, S. *J. Am. Chem. Soc.* **2011**, *133*, 11692.
- (46) Ohzu, S.; Ishizuka, T.; Hirai, Y.; Jiang, H.; Sakaguchi, M.; Ogura, T.; Fukuzumi, S.; Kojima, T. *Chem. Sci.* **2012**, *3*, 3421.
- (47) Ishizuka, T.; Ohzu, S.; Kotani, H.; Shiota, Y.; Yoshizawa, K.; Kojima, T. *Chem. Sci.* **2014**, *5*, 1429.
- (48) Dhuri, S. N.; Seo, M. S.; Lee, Y.-M.; Hirao, H.; Wang, Y.; Nam, W.; Shaik, S. *Angew. Chem., Int. Ed.* **2008**, *47*, 3356.
- (49) Groves, J. T. *J. Chem. Edu.* **1985**, *62*, 928.
- (50) Groves, J. T. *Proc. Natl. Acad. Sci. U.S.A.* **2003**, *100*, 3569.
- (51) Groves, J. T. *J. Inorg. Biochem.* **2006**, *100*, 434.
- (52) Shaik, S.; Kumar, D.; de Visser, S. P.; Altun, A.; Thiel, W. *Chem. Rev.* **2005**, *105*, 2279.
- (53) Ortiz de Montellano, P. R. *Chem. Rev.* **2010**, *110*, 932.
- (54) Cho, K.-B.; Wu, X.; Lee, Y.-M.; Kwon, Y. H.; Shaik, S.; Nam, W. *J. Am. Chem. Soc.* **2012**, *134*, 20222.
- (55) Wu, X.; Seo, M. S.; Davis, K. M.; Lee, Y.-M.; Chen, J.; Cho, K.-B.; Pushkar, Y. N.; Nam, W. *J. Am. Chem. Soc.* **2011**, *133*, 20088.
- (56) Cho, K.-B.; Shaik, S.; Nam, W. *J. Phys. Chem. Lett.* **2012**, *3*, 2851.
- (57) Cho, K.-B.; Kang, H.; Woo, J.; Park, Y. J.; Seo, M. S.; Cho, J.; Nam, W. *Inorg. Chem.* **2014**, *53*, 645.
- (58) Kwon, E.; Cho, K.-B.; Hong, S.; Nam, W. *Chem. Commun.* **2014**, *50*, 5572.
- (59) Kwon, Y. H.; Mai, B. K.; Lee, Y.-M.; Dhuri, S. N.; Mandal, D.; Cho, K.-B.; Kim, Y.; Shaik, S.; Nam, W. *J. Phys. Chem. Lett.* **2015**, *6*, 1472.
- (60) Concepcion, J. J.; Tsai, M.-K.; Muckerman, J. T.; Meyer, T. J. *J. Am. Chem. Soc.* **2010**, *132*, 1545.
- (61) Evans, D. F. *J. Chem. Soc.* **1959**, 2003.
- (62) Evans, D. F.; Jakubovic, D. A. *J. Chem. Soc., Dalton Trans.* **1988**, 2927.
- (63) Eckart, C. *Phys. Rev.* **1930**, *35*, 1303.
- (64) Moyer, B. A.; Sipe, B. K.; Meyer, T. J. *Inorg. Chem.* **1981**, *20*, 1475.
- (65) Concepcion, J. J.; Jurss, J. W.; Templeton, J. L.; Meyer, T. J. *J. Am. Chem. Soc.* **2008**, *130*, 16462.
- (66) Swavey, S.; Fang, Z.; Brewer, K. J. *Inorg. Chem.* **2002**, *41*, 2598.
- (67) Saltzman, H.; Sharefkin, J. G. *Organic Syntheses, Collection Volume V*; Wiley: New York, 1973.
- (68) Armarego, W. L. F.; Chai, C. L. L. *Purification of Laboratory Chemicals*, 6th ed.; Pergamon Press, Oxford, U.K., 2009.
- (69) Luo, Y.-R. *Handbook of Bond Dissociation Energies in Organic Compounds*; CRC Press: New York, 2002.
- (70) Kohn, W.; Sham, L. J. *Phys. Rev.* **1965**, *140*, A1133.
- (71) Becke, A. D. *Phys. Rev. A* **1988**, *38*, 3098.
- (72) Becke, A. D. *J. Chem. Phys.* **1993**, *98*, 1372.
- (73) Becke, A. D. *J. Chem. Phys.* **1993**, *98*, 5648.
- (74) Lee, C.; Yang, W.; Parr, R. G. *Phys. Rev. B* **1988**, *37*, 785.
- (75) Hay, P. J.; Wadt, W. R. *J. Chem. Phys.* **1985**, *82*, 299.
- (76) Francl, M. M.; Pietro, W. J.; Hehre, W. J.; Gordon, M. S.; DeFrees, D. J.; Pople, J. A. *J. Chem. Phys.* **1982**, *77*, 3654.
- (77) Frisch, M. J.; Trucks, G. W.; Schlegel, H. B.; Scuseria, G. E.; Robb, M. A.; Cheeseman, J. R.; Scalmani, G.; Barone, V.; Mennucci, B.; Petersson, G. A.; Nakatsuji, H.; Caricato, M.; Li, X.; Hratchian, H. P.; Izmaylov, A. F.; Bloino, J.; Zheng, G.; Sonnenberg, J. L.; Hada, M.; Ehara, M.; Toyota, K.; Fukuda, R.; Hasegawa, J.; Ishida, M.; Nakajima, T.; Honda, Y.; Kitao, O.; Nakai, H.; Vreven, T.; Montgomery, J. A.; Peralta, J. E.; Ogliaro, F.; Bearpark, M.; Heyd, J. J.; Brothers, E.; Kudin, K. N.; Staroverov, V. N.; Kobayashi, R.; Normand, J.; Raghavachari, K.; Rendell, A.; Burant, J. C.; Iyengar, S. S.; Tomasi, J.; Cossi, M.; Rega, N.; Millam, J. M.; Klene, M.; Knox, J. E.; Cross, J. B.; Bakken, V.; Adamo, C.; Jaramillo, J.; Gomperts, R.; Stratmann, R. E.; Yazyev, O.; Austin, A. J.; Cammi, R.; Pomelli, C.; Ochterski, J. W.; Martin, R. L.; Morokuma, K.; Zakrzewski, V. G.; Voth, G. A.; Salvador, P.; Dannenberg, J. J.; Dapprich, S.; Daniels, A. D.; Farkas, Foresman, J. B.; Ortiz, J. V.; Cioslowski, J.; Fox, D. J. *Gaussian 09, Revision D.01*, 2009.

- 1
2
3 (78) Cossi, M.; Rega, N.; Scalmani, G.; Barone, V. *J. Comput. Chem.* **2003**, *24*, 669.
- 4 (79) Weigend, F.; Ahlrichs, R. *Phys. Chem. Chem. Phys.* **2005**, *7*, 3297.
- 5 (80) Yamaguchi, K.; Jensen, F.; Dorigo, A.; Houk, K. N. *Chem. Phys. Lett.* **1988**, *149*, 537.
- 6 (81) Grimme, S.; Ehrlich, S.; Goerigk, L. *J. Comput. Chem.* **2011**, *32*, 1456.
- 7 (82) Winget, P.; Cramer, C. J.; Truhlar, D. G. *Theor. Chem. Acc.* **2004**, *112*, 217.
- 8 (83) Mandal, D.; Ramanan, R.; Usharani, D.; Janardanan, D.; Wang, B.; Shaik, S. *J. Am. Chem. Soc.* **2015**, *137*, 722.
- 9 (84) Duncan, W. T.; Bell, R. L.; Truong, T. N. *J. Comput. Chem.* **1998**, *19*, 1039.
- 10 (85) Harvey, J. N.; Aschi, M.; Schwarz, H.; Koch, W.; *Theor. Chem. Acc.* **1998**, *99*, 95.
- 11
12
13
14
15
16
17
18
19
20
21
22
23
24
25
26
27
28
29
30
31
32
33
34
35
36
37
38
39
40
41
42
43
44
45
46
47
48
49
50
51
52
53
54
55
56
57
58
59
60

Table of Contents Graphic

